DOI: 10.1039/c6cp08078b

Tuning the ambipolar charge transport properties of tricyanovinyl-substituted carbazole-based materials

Marta Reig,[a] Gintautas Bagdziunas [¥] [b] Dmytro Volyniuk,[b] Juozas V. Grazulevicius[b] and Dolores Velasco*[a]

Abstract: A series of push-pull carbazole-based compounds has been experimentally and theoretically characterized in combination with the X-ray analysis of the corresponding single crystals. The introduction of the strong electron-withdrawing tricyanovinyl group in the carbazole core affords electron-transporting ability in addition to the characteristic hole-transporting properties exhibited by donor carbazole derivatives.

Introduction

Organic electroactive molecular materials offer many advantages for electronic and optoelectronic devices, such as low cost, capability of forming thin films which enable fabrication of large-area and flexible devices. In addition, simple purification and characterization metods can be used due to their small size and well defined structure.[1]
In the field of organic electronics, both p- and n-type organic semiconductors are required for device fabrication. In terms of charge mobility and air stability, the development and performance of p-type semiconducting materials has been higher relative to the n-type counterparts. Therefore, research efforts are currently focused on the search of new n-type or ambipolar semiconducting materials.[2] For the design of new n-type organic semiconductors, materials with high electron affinities to facilitate charge injection and ambient stability are required[ref]. Energy levels and band gaps of small organic molecules can be easily modulated by the design of appropriate charge-transfer compounds. The push-pull electronic structure generates low band gap materials with the possibility to control the HOMO and LUMO energetic levels.[3]
Incorporation of the strong electron-withdrawing tricyanovinyl group in push-pull organic compounds has been explored in combination with various π-systems giving promising materials for organic electronics.[4-7] This work is focused on a series of push-pull compounds containing tricyanovinyl and carbazole fragments. Carbazole derivatives are well-known hole-transporting materials,[8] due to the electron-donating capability of the carbazole unit. The carbazole moiety posses a series of advantages relative to other building blocks of organic electroactive materials.[9] Firstly, carbazole is a cheap and easily available product. Secondly, it is a highly stable compound in the different chemical and environmental conditions due to its fully aromatic configuration[ref]. Moreover, the nitrogen atom and 3,6 positions can be easily chemically substituted with a wide variety of functional groups in order to modulate the optical and the electrical, glass-forming properties.[10]
Carbazole derivatives incorporating the tricyanovinyl group have been previously reported showing high nonlinear optical (NLO) responses,[4] but to the best of our knowledge the charge transport properties of this type of materials are not yet reported. Here we focus on the modification of the charge-transporting properties of the carbazole derivatives by the introduction of the strong electron-withdrawing tricyanovinyl group affording a push-pull system with high electron affinity. The electron-donating nature of the carbazole unit was modulated by alkylation of the nitrogen atom and by the introduction of the electron-donating methoxy group in the *ortho* position with respect to the tricyanovinyl fragment. The effect of the substitution patterns of the carbazole core in terms of thermal, optical, electrochemical and charge-transporting properties is here reported. Single crystal X-ray analysis and theoretical calculations gave insight into the relationship between the molecular structure of the organic semiconductors and the charge mobilities.

[a] M. Reig, Dr. D. Velasco
Grup de Materials Orgànics
Institut de Nanociència i Nanotecnologia (IN^{2}UB)
Departament de Química Inorgànica i Orgànica
Secció de Química Orgànica
Universitat de Barcelona
Martí i Franquès, 1, 08028 Barcelona (Spain)
E-mail: dvelasco@ub.edu
[b] Dr. G. Bagdžiūnas[¥], Dr. D. Volyniuk, Dr. J. V. Grazulevicius
Department of Polymer Chemistry and Technology
Kaunas University of Technology
Radvilenu pl. 19, 50254 Kaunas (Lithuania)
[¥] Present address: State Research Centre for Physical Sciences and Technology, Sauletekio av. 3, 10257 Vilnius (Lithuania)

Supporting information for this article is given via a link at the end of the document.

DOI: 10.1039/c6cp08078b

Results and Discussion

Scheme 1 displays the preparation of the series of tricyanovinyl-containing compounds: 3-(1,2,2-tricyanovinyl)-9*H*-carbazole (**1**), 2-methoxy-3-(1,2,2-tricyanovinyl)-9*H*-carbazole (**2**), 9-methyl-3-(1,2,2-tricyanovinyl)-9*H*-carbazole[4a] (**3**) and 2-methoxy-9-methyl-3-(1,2,2-tricyanovinyl)-9*H*-carbazole (**4**). The key synthetic step is the introduction of the strong tricyanovinyl electron-withdrawing group into the electron rich carbazole unit. Compounds **1**-**4** were obtained in a simple and direct method by heating the corresponding carbazole precursor with tetracyanoethylene in anhydrous *N*,*N*-dimethylformamide (DMF) at 50 °C. Tricyanovinyl derivative **1** was prepared from

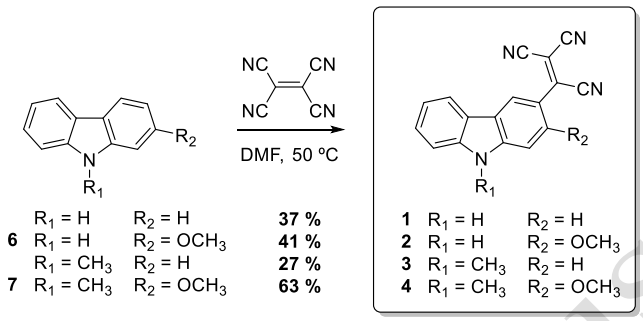

Scheme 1. Synthesis of tricyanovinyl derivatives **1**-**4**.

9*H*-carbazole, whereas **3** was prepared after methylation under standard conditions of 9*H*-carbazole. Tricyanovinyl-based compounds **2** and **4** were synthesized from 2-methoxy-9*H*-carbazole[11] (**6**) and 9-methyl-2-methoxy-9*H*-carbazole[12] (**7**), respectively. Compound **6** was obtained through an alternative methodology consisting of a two- step process (Scheme 2). Firstly, the Suzuki coupling reaction of 1-bromo-2-nitrobenzene with 4-methoxyphenylboronic acid afforded the intermediate 4'-methoxy-2-nitro-1,1'-biphenyl (**5**). Secondly, the Cadogan cyclization reaction of **5** with triethyl phosphite gave compound **6** that rendered **7** after a methylation process under standard conditions.

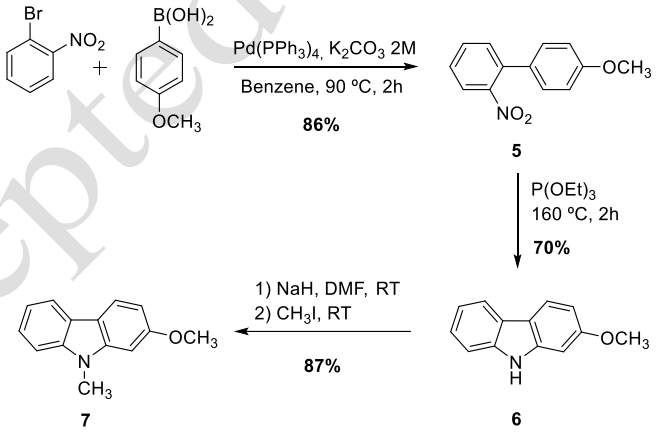

Scheme 2. Synthesis of 2-methoxy-9*H*-carbazole intermediates **6** and **7**.

All the compounds were entirely characterized by ^{1}H NMR and ^{13}C NMR spectroscopies and mass spectrometry. The crystal structures of compounds **3** and **4** were determined by single-crystal X-ray analysis. Suitable single crystals were grown by slow evaporation from the corresponding chloroform solutions. Figure 1 shows the Oak Ridge Thermal Ellipsoid Plot (ORTEP) projections of molecules **3** and **4**. The detailed crystallographic data can be found in the Supporting Information.

DOI: 10.1039/c6cp08078b

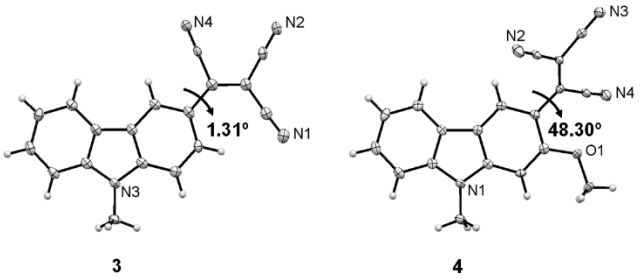

Figure 1. X-ray crystal structures of molecules **3** and **4**, showing the 50% probability displacement.

The introduction of the methoxy group in the *ortho* position with respect to the tricyanovinyl unit influences the twist angle between the tricyanovinyl and the carbazole planes. Whereas molecule **3** containing no methoxy substituent adopts an almost planar conformation with an angle of 1.31°, the *ortho*-methoxy-substituted analogue **4** shows a deviation of the planarity with a twist angle of 48.30°, because of the steric hindrance caused by the methoxy group.

Thermogravimetric analysis (TGA) and differential scanning calorimetry (DSC) measurements were performed to investigate the thermal properties of carbazole derivatives **1**-**4** (Table 1 and Supporting Information). All the compounds possess high thermal stabilities with high onset decomposition temperatures in the range of 248 to 305 °C. DSC thermograms confirmed the crystalline nature of this series of tricyanovinyl derivatives. *N*-Methyl derivatives **3** and **4** showed a melting process during the first heating scan together with an exothermic peak during the cooling scan owing to the crystallization process, whereas the non-alkylated analogues **1** and **2** melted with decomposition.

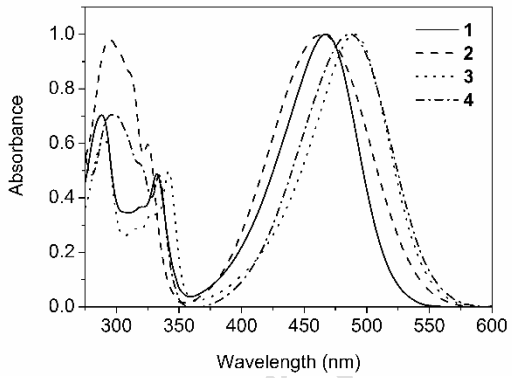

Figure 2. UV-vis absorption spectra of 10 μM solutions of compounds **1**-**4** in dichloromethane.

Table 1. Thermal and optical properties for tricyanovinyl-substituted carbazole derivatives **1**-**4**.

Compd.	T_d [a] (°C)	T_m [b] (°C)	T_c [b] (°C)	$\lambda_{abs,max}$ (nm)[c] [ε (mol^{-1} dm^3 cm^{-1})]
1	289	309	-	288 (19 040), 466 (27 030)
2	248	255	-	295 (19 159), 464 (19 580)
3	301	245	231	290 (19 660), 490 (35 090)
4	305	249	197	296 (15 970), 486 (22 630)

[a] Onset decomposition temperature (T_d) obtained from TGA performed at a heating rate of 20 °C min^{-1}. [b] Melting point (T_m) and crystallization temperature (T_c) obtained from DSC performed at a scan rate of 10 °C min^{-1}. [c] Measured in 10 μM dichloromethane solutions at room temperature.

The UV-vis absorption spectra of 10 μM dichloromethane solutions of compounds **1**-**4** are shown in Figure 2 and the corresponding optical data is collected in Table 1. All compounds exhibit similar absorption spectra with absorption in the UV zone with a maximum peaking around 288-296 nm, characteristic of the carbazole moiety, and a second broad and intense absorption band centred in the range of 464 to 490 nm, which is assigned to the intramolecular charge transfer from the electron-donating carbazole moiety to the electron-withdrawing tricyanovinyl group. *N*-Alkyl derivatives **3** and **4** show a red-shift of the charge transfer absorption band of 24 and 22 nm, respectively, in comparison to the non-alkylated counterparts **1** and **2**. The strong donor-acceptor configuration of these molecules allows the coverage of the UV and the visible region of the electromagnetic spectrum.

DOI: 10.1039/c6cp08078b

Electrochemical properties were investigated by cyclic voltammetry (Table 2 and Supporting Information). Compounds **1**-**4** show two reduction waves, being the first one *quasi*-reversible and the second one irreversible, together with an irreversible oxidation wave. Consistent with the strong electron-donating capability of the 2-methoxy group, compounds 2-methoxy substituted **2** and **4** are less easily reduced and more easily oxidized, exhibiting lower electron affinity (EA) and ionization potential (IP) values, than the non-substituted counterparts **1** and **3**. Ionization potentials and electron affinities range between 6.34-6.46 and 4.32-4.40 eV, respectively. The amphoteric redox properties indicate the potential behaviour of this series of compounds for both hole and electron transport.

The structures of compounds **1**-**4** were explored by full optimization of the molecular structure by density functional theory (DFT) calculations in vacuum. The twist angles between the tricyanovinyl and carbazole planes of the optimized molecular structures were calculated to be 19.7° and 41.0° for **3** and **4**, respectively. The difference between the above-mentioned twist angles with those of the crystal forms (1.31° and 48.3° for **3** and **4**, respectively) could be attributed to the presence of intermolecular interactions between molecules in the solid state.

The highest occupied molecular orbitals (HOMO) are mainly localized at the electron rich carbazole moiety with some contribution of the tricyanovinyl and the methoxy moieties, evidencing their influence on the energy of the HOMO (Figure 3). Compounds **2** and **4** show the highest values of theoretical HOMO

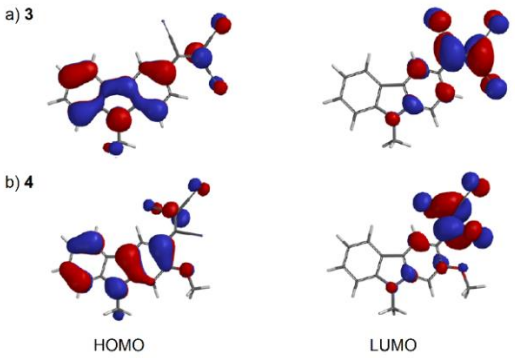

Figure 3. Computed spatial distributions of HOMO and LUMO orbitals of a) **3** and b) **4** (isovalue is 0.032).

levels (i.e. -6.43 and -6.37 eV, respectively) due to the attached electron-donating methoxy group (Table 2). These values follow the same trend and are close (±0.2 eV) to the IP values obtained from the electrochemical measurements (Table 2). The efficient withdrawing effect of the tricyanovinyl moiety leads to localization of the lowest unoccupied molecular orbital (LUMO) mainly on the tricyanovinyl group. Compounds **1** and **3**, without the methoxy substitution, exhibit the lowest LUMO energy values.

Table 2. Electrochemical properties for tricyanovinyl-substituted carbazole derivatives **1**-**4**.

Compound	$E^{0}_{red,1}$ (V)[a]	E^{red}_{onset} (V)[b]	E^{ox}_{onset} (V)[b]	EA (V)[c]	IP (V)[c]	E_{gap}[c]	$-E^{DFT}_{HOMO}$ (eV)[d]	$-E^{DFT}_{LUMO}$ (eV)[d]
1	-1.07	-0.99	1.07	4.40	6.46	2.06	6.64	3.68
2	-1.14	-1.06	0.95	4.33	6.34	2.01	6.43	3.51
3	-1.08	-1.00	1.06	4.39	6.45	2.06	6.50	3.62
4	-1.14	-1.07	0.98	4.32	6.37	2.05	6.37	3.47

[a] Standard potential of the first reduction redox couple ($E^{0}_{red,1}$) and [b] onset reduction potential (E^{red}_{onset}) and onset oxidation potential (E^{ox}_{onset}) vs. Fc^{+}/Fc estimated from cyclic voltammetries of 1 mM dichloromethane solutions at a scan rate of 100 mV s^{-1}. [c] Estimated from cyclic voltammetries as EA = $E^{red}_{onset\ vs.\ Fc+/Fc}$ + 5.39, IP = $E^{ox}_{onset\ vs.\ Fc+/Fc}$ + 5.39 and E_{gap} = IP - EA. [d] Estimated HOMO and LUMO values by B3LYP/6-31+G(d).

DOI: 10.1039/c6cp08078b

The relationship between the HOMO/LUMO energy, or probability of the band gaps engineering between the frontier molecular orbitals, and the rotation probability of the tricyanovinyl group in the neutral, cationic and anionic states of molecules **3** and **4** were estimated using the potential energy surfaces (PES) scans. The PES scans of the neutral, cationic and anionic sates of molecules **3** and **4** were conducted by rotating the tricyanovinyl moiety in steps of 20° from 0 to 360°. The rotation barriers for **3** and **4** were estimated to be of 23 and 14 kJ mol^{-1}, respectively. The PES scans are depicted in the Supporting Information.

The charge transport properties of the vacuum-evaporated layers of compounds **1**-**4** were studied by the time-of-flight (TOF) technique (Table 3). The attachement of the strong electron-withdrawing tricyanovinyl group to the carbazole moiety impacts on the charge transporting properties and as a result electron transport is observed in the layers of these carbazole-based compounds. Representative TOF transients for electron transport of compound **2** are displayed in Figure 4. TOF transients and the dependency of hole and electron drift mobilities on the square root of the electric field for this series of compounds are collected in the Supporting Information. Transient curves in the linear scale for all compounds show a dispersive pattern. Nevertheless, transit times could be determined in the log-log scale.

Table 3. Hole and electron mobility data for the layers of tricyanovinyl-based compounds **1**-**4** obtained by the TOF technique.

	Electrons			Holes		
Compound	μ_e ($cm^2\ V^{-1}\ s^{-1}$) [F ($V\ cm^{-1}$)] [a]	μ_0 ($cm^2\ V^{-1}\ s^{-1}$) [b]	α ($cm\ V^{-1}$)$^{1/2}$ [c]	μ_h ($cm^2\ V^{-1}\ s^{-1}$) [F ($V\ cm^{-1}$)] [a]	μ_0 ($cm^2\ V^{-1}\ s^{-1}$) [b]	α ($cm\ V^{-1}$)$^{1/2}$ [c]
1	2.6×10^{-4} [4.8×10^5]	6.4×10^{-7}	0.0087	-	-	-
2	3.1×10^{-5} [9.5×10^5]	2.3×10^{-8}	0.0072	1.8×10^{-4} [9.5×10^5]	4.4×10^{-7}	0.0061
3	7.2×10^{-4} [4.0×10^5]	1.3×10^{-4}	0.0027	-	-	-
4	9.3×10^{-5} [7.1×10^5]	2.6×10^{-6}	0.0042	2.4×10^{-4} [7.1×10^5]	7.2×10^{-6}	0.0042

[a] Electron (μ_e) and hole (μ_h) mobilities at the corresponding electric field (F). [b] Zero-field mobilities (μ_0). [c] Field dependences (α). Measurements were determined in air and at room temperature. The thickness of the vacuum evaporated layers varied from 0.8 to 5.0 μm.

DOI: 10.1039/c6cp08078b

The layers of tricyanovinyl derivatives **1** and **3**, showed only electron transport. *N*-methyl-substituted compound (**3**) exhibited the the highest electron mobility of all the series of 7.2×10^{-4} cm^2 V^{-1} s^{-1}. Hole transport was not detected in the layers of these compounds by TOF technique. Remarkably, the introduction of the electron-donating methoxy group in the *ortho* position with respect to the tricyanovinyl fragment in compounds **2** and **4** afforded the ambipolar properties. The *N*-alkylated derivative **4** showed more balanced electron and hole mobilities of 9.3×10^{-5} and 2.4×10^{-4} cm^2 V^{-1} s^{-1}, respectively, than the non-alkylated analogue **2**.

In order to gain insight into the fundamentals of the relationship between the chemical structure and the above mentioned electrical properties of this series of compounds, DFT calculations were performed. In a first instance, the reorganization energies (λ) for holes and electrons were estimated for compounds **3** and **4**. The reorganization energy may be defined as the relaxation energy of a molecule from the geometry of the neutral state to the charged (anion and cation) state and from the charged to the neutral state. The reorganization energies in vacuum for holes (λ_+) were calculated to be 75.4 and 289 meV and for electrons (λ_-) 344 and 352 meV were estimated for **3** and **4**, respectively. From PES analysis, the tricyanovinyl moiety vibrations for all states of **3** and **4** within the intervals of twist angles from -40° to +40° for **3**, and -60° to -30° together with 30° to 60° for **4** are possible in vacuum at room temperature, due to the rotation barriers at those intervals are lower than the thermal energy $k_bT = 2.48$ kJ mol^{-1}, where k_b is the Boltzmann constant and T is the temperature (Supporting Information).

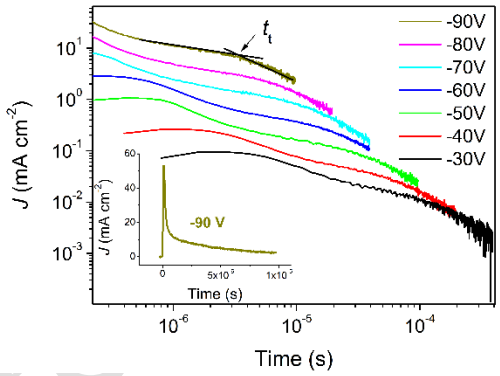

Figure 4. TOF transients for electron transport for compound **2**. Inset shows one of the transient curves in the linear plot.

DOI: 10.1039/c6cp08078b

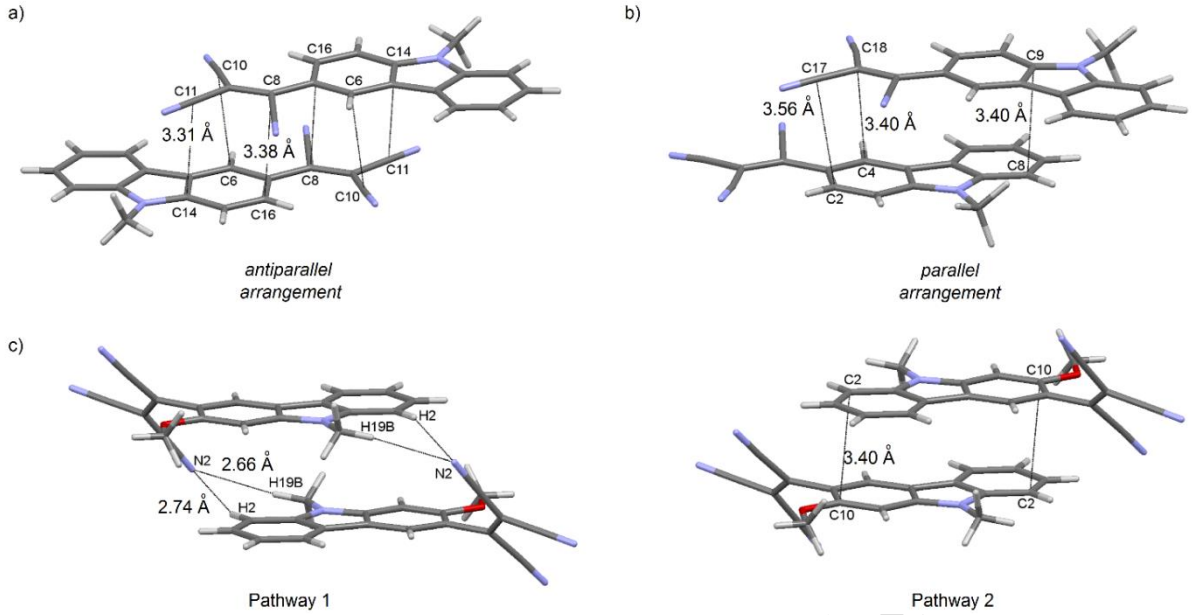

Figure 5. Selected carrier hopping pathways between neighbouring molecules and intermolecular interactions for a) the here reported crystal structure of **3**, b) the previously reported crystal structure[14] of **3** and c) **4**.

DOI: 10.1039/c6cp08078b

However, it should be mentioned that the structures of molecules **3** and **4** in the solid state are different than those predicted in vacuum, because the rotation of the lateral groups should be fixed by intermolecular forces. Indeed, Vaissier et al.[13] showed that performing DFT calculations on the isolated molecules systematically underestimates the energy barrier to charge transfer, which is important to take into consideration when designing conductive molecular materials. Taking into account the twist angles obtained from the single crystal structures (i.e. 1.31° for **3** and 48.3° for **4**, Figure 1) for the solid state, the calculation of the reorganization energies was carried out again as previously, showing values for holes (λ_+) of 64.4 and 249 meV and for electrons (λ_-) of 310 and 369 meV for **3** and **4**, respectively, following the same trend as the obtained values estimated in vacuum. Thus, the calculated reorganization energies for holes and electrons are similar for the methoxy-substituted derivative **4**, but differ considerably for compound **3**, pointing to an expected more balanced charge transport characteristics for the layers of compound **4**.

Charge mobilities of compounds **3** and **4** were theoretically estimated in order to establish the relationship between the molecular origin and the different hole and electron transport behaviour across layers of compounds **3** and **4** determined by the TOF technique. For this purpose, the crystal structures of **3** and **4** were used to generate a wide variety of possible hopping pathways between neighbouring molecules with intermolecular interactions as it is shown in Figure 5 and in the Supporting Information. It should be mentioned that the crystal structure of compound **3** presented in this work is different from the one previously reported.[14] Therefore, both structures have been considered for the determination of the hopping pathways. According to the Holstein small polaron limit, a charge is localized on a single organic molecule[ref]. The rate of charge transfer between molecules was estimated by the Marcus theory[ref]. All data of charge mobility calculations are summarized in the Supporting Information (Table S3) and the details of the theoretical calculations are given in the experimental section.

The carrier hopping pathways shown in Figure 5 for compounds **3** and **4** were considered to be the most effective and they were selected for the charge carrier mobility calculations. Compounds **3** and **4** exhibit a layered organization. Neighbouring molecules of **3** from the here and the already reported English crystal structure[14] are interlinked via $\pi\cdots\pi$ interactions to produce antiparallel and parallel arrangements, respectively, showing the strongest intermolecular interactions among all the proposed pathways, with interaction energies of -111 and -76.9 kJ mol^{-1}, respectively. Hence, these two carrier hopping pathways, from the here and the already reported crystal structure[14] of **3**, were considered for the charge carrier mobility calculations. On the other hand, for compound **4**, among all the considered pathways (Figure 5c and Figure S10 in the Supporting Information), only pathway 1 and 2 were taken into account for the charge carrier mobility calculations due to the significant site probabilities of 0.76 and 0.24, respectively. Adjacent molecules in pathways 1 and 2 are connected via C-H···NC hydrogen bonding and $\pi\cdots\pi$ interactions to produce an antiparallel arrangement, showing the highest interaction energies of -99.7 and -96.8 kJ mol^{-1}, respectively, among all the proposed pathways.

For the selected pathways shown in Figure 5 from the here and the already reported crystal structure[14] of compound **3**, the calculated coupling integral values for electrons were found to be higher (140 and 166 meV) than for holes (47.4 and 83.2 meV, respectively), pointing out that for compound **3** electron transport is favoured relative to hole transport. On the other hand, for

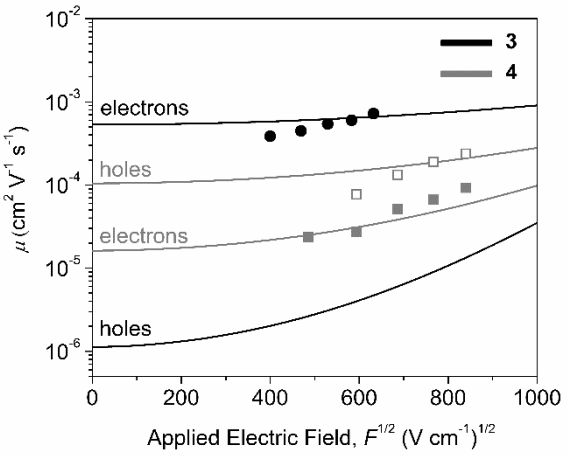

Figure 6. Visualization of the experimental (symbols) and predicted (lines) charge mobilities of **3** and **4.**

DOI: 10.1039/c6cp08078b

compound 4, the coupling integrals for pathway 1, which showed the highest site probability value, were estimated to be 21.8 for electrons and 63.1 for holes, respectively, indicating that for compound **4** hole transport is more favoured.

The thickness of the vacuum evaporated layers ranged from 0.8 to 5.0 μm that corresponds to the distance between the electrodes. The possible quantity of charge hopping was estimated to be $10^{4\pm1}$ considering the distances between the neighbouring donor-donor (D-D) and acceptor-acceptor (A-A) moieties determined from the crystal structures (Table S3 in the Supporting Information). Taking into account this data, the probability cut off was of 10^{-5} for the charge mobility calculations. The calculated mobility dependence on the applied electric field for the modelled layers shows a good qualitative agreement with the data obtained from TOF experiments (Figure 6). The experimental and theoretical charge mobilities of electrons for 3 at the highest experimental electric field of 4.0×10^5 V cm^{-1} were determined and calculated to be 7.2×10^{-4} and 6.6×10^{-4} cm^2 V^{-1} s^{-1}, respectively. Whereas hole mobilities for compound **3** were not detected by the experimental TOF method. They were predicted via our theoretical model to be very low on the order of 10^{-6} cm^2 V^{-1} s^{-1}. For compound **4**, the experimental and theoretical charge mobilities of holes and electrons at the highest experimental electric field of 7.1×10^5 V cm^{-1} were estimated to be 2.4×10^{-4}/2.1×10^{-4} for holes and 9.3×10^{-5}/5.8×10^{-5} cm^2 V^{-1} s^{-1} for electrons, respectively.

The presented results suggest that the charge transport throughout layers of compounds **1-4** depend considerably on the supramolecular organization, which is highly influenced by the *ortho*-methoxy substituent on the carbazole core with respect to the tricyanovinyl group. Indeed, the tricyanovinyl fragment in compound **4** is placed out of the molecular plane due to the steric hindrance caused by the methoxy fragment. Taking into account that the HOMO is localized mainly at the electron rich carbazole moiety for both **3** and **4** compounds (Figure 3), the twisted structure of compound **4** implies a face-to-face interaction between adjacent donor carbazole fragments that enhances the overlap between HOMO-HOMO orbitals, in contrast to the planar structure of compound **3** with slipped cofacial interactions between the adjacent donor carbazole units (Figure 5). From the charge transport point of view, the enhanced intermolecular π-orbital overlap between adjacent donor moieties in the *ortho*-methoxy substituted compound **4** could explain the enhancement of the hole mobility observed for **4** in comparison to that recorded for **3**. On the other hand, considering that the LUMO is mainly localized in the tricyanovinyl unit, a greater overlap between LUMOs of neighbouring molecules is expected for the planar compound **3** than for compound **4**, since the accepting tricyanovinyl groups of neighbouring molecules are closer in compound **3** (Figure 5 and Table S3 of the Supporting Information). This feature is corroborated with the higher calculated coupling integral values for electrons for compound **3** with respect to that for holes. Accordingly, compound **3** showed the highest electron mobilities observed both experimentally and theoretically.

Conclusions

The charge transport properties of a series of push-pull carbazole-based compounds bearing the strong electron-withdrawing tricyanovinyl group have been examined. All the compounds exhibited high thermal stability and charge-transfer absorption bands in the visible region, together with hole and electron transport ability due to the amphoteric redox properties. TOF measurements confirm that the substitution of the carbazole core with the electron-withdrawing tricyanovinyl group is a useful strategy to achieve electron transporting materials. *N*-Alkylated derivatives **3** and **4** showed enhanced charge transport properties in comparison to the non-alkylated analogues **1** and **2**. In addition, ambipolar properties could be detected by the TOF technique by the additional incorporation of the electron-donating methoxy group in the *ortho* position with respect to the tricyanovinyl fragment. In this way, almost balanced electron and hole mobilities of 9.3×10^{-5} and 2.4×10^{-4} cm^2 V^{-1} s^{-1}, respectively, were attained for compound **4** at high electric fields under ambient conditions, whereas the non-methoxy substituted carbazole derivatives **1** and **3** exhibited exclusively electron transport. Although, the electron-donating methoxy substituent might modulate the charge-transporting properties, as well as the HOMO and LUMO levels, by controlling the donor strength of the carbazole core and the molecular planarity, the analysis of the single-crystal structures by X ray analysis together with the theoretical calculations suggest that the charge transport properties of the layers of this series of push-pull derivatives are highly influenced by the supramolecular organization. The planar structures of compounds **1** and **3** favour LUMO-LUMO interactions between neighbouring molecules, resulting in the enhancement of the electron transport. On the contrary, the twisted structures of compounds **2** and **4** induce more effective face-to-face $\pi\cdots\pi$ interactions between adjacent donor carbazole moieties, which can be related to the more extended interaction between HOMO-HOMO orbitals, and consequently hole transport is favoured without losing the electron-transporting properties.

DOI: 10.1039/c6cp08078b

Experimental Section

Materials

All chemicals were of commercial grade and used as received. 9-Methyl-3-(1,2,2-tricyanovinyl)-9*H*-carbazole (**3**) was synthesized as already reported.[4a]

Synthesis of 3-(1,2,2-tricyanovinyl)-9*H*-carbazole (1)

9*H*-Carbazole (300 mg, 1.79 mmol) was dissolved in 10 mL of anhydrous DMF under nitrogen atmosphere. Then, tetracyanoethylene (284 mg, 2.22 mmol) was added and the solution was stirred at 50 °C for 52 h. The cooled mixture was poured into a water/ice solution and the product was extracted with ethyl acetate. The organic layer was dried over Na_2SO_4, filtered off and the solvent was distilled off under reduced pressure. The crude was purified by flash column chromatography by using a mixture of hexane and ethyl acetate (3:1 v/v) as the eluent to give compound **1** as a red solid (176 mg; 37%). ^{1}H NMR (400 MHz, Acetone-d_6): δ = 11.27 (s, 1H), 8.94 (d, J = 2.0 Hz, 1H), 8.32 (d, J = 7.9 Hz, 1H), 8.21 (dd, J = 8.8 Hz, J = 2.0 Hz, 1H), 7.82 (d, J = 8.8 Hz, 1H), 7.67 (d, J = 8.2 Hz, 1H), 7.58-7.54 (m, 1H), 7.39-7.35 ppm (m, 1H); ^{13}C NMR (100 MHz, DMSO-d_6): δ = 143.9, 140.7, 140.7, 127.7, 126.9, 123.9, 123.3, 122.0, 121.1, 121.0, 119.7, 115.0, 113.4, 113.3, 112.6, 112.2, 86.3 ppm; HRMS (ESI-MS): *m/z*: calcd for $C_{17}H_9N_4$: 269.0822 $(M+H)^+$; found: 269.0818.

Synthesis of 2-methoxy-3-(1,2,2-tricyanovinyl)-9*H*-carbazole (2)

6 (300 mg, 1.52 mmol) was dissolved in 10 mL of anhydrous DMF under a nitrogen atmosphere. Then, tetracyanoethylene (241 mg, 1.88 mmol) was added and the solution was stirred at 50 °C for 48 h. The cooled mixture was poured into a water/ice solution and the product was extracted with ethyl acetate. The organic layer was dried over Na_2SO_4, filtered off and the solvent was distilled off under reduced pressure. The crude was purified by flash column chromatography by using a mixture of hexane and dichloromethane (1:4 v/v) as the eluent to give compound **2** as a red solid (185 mg; 41%). ^{1}H NMR (400 MHz, Acetone-d_6): δ = 10.91 (s, 1H), 8.58 (s, 1H), 8.14 (d, J = 7.8 Hz, 1H), 7.55 (d, J = 8.1 Hz, 1H), 7.45-7.41 (m, 1H), 7.31 (s, 1H), 7.30-7.26 (m, 1H), 4.09 ppm (s, 3H); ^{13}C NMR (100 MHz, DMSO-d_6): δ = 156.9, 145.7, 140.6, 138.4, 126.3, 124.2, 122.2, 120.6, 120.0, 117.2, 114.6, 112.9, 112.5, 111.7, 110.6, 94.2, 91.6, 56.3 ppm; HRMS (ESI-MS): *m/z*: calcd for $C_{18}H_9N_4O$: 297.0782 $(M-H)^-$; found: 297.0784.

Synthesis of 2-methoxy-9-methyl-3-(1,2,2-tricyanovinyl)-9*H*-carbazole (4)

7 (380 mg, 1.80 mmol) was dissolved in 10 mL of anhydrous DMF under a nitrogen atmosphere. Then, tetracyanoethylene (297 mg, 2.32 mmol) was added and the solution was stirred at 50 °C for 72 h. The cooled mixture was poured into a water/ice solution and the product was extracted with ethyl acetate. The organic layer was dried over Na_2SO_4, filtered off and the solvent was distilled off under reduced pressure. The crude was purified by flash column chromatography by using a mixture of hexane and dichloromethane (1:1 v/v) as the eluent to give compound **4** as a dark green solid (353 mg; 63%). ^{1}H NMR (400 MHz, DMSO- d_6): δ = 8.57 (s, 1H), 8.10 (d, J = 7.7 Hz, 1H), 7.64 (d, J = 8.2 Hz, 1H), 7.53-7.49 (m, 1H), 7.44 (s, 1H), 7.33-7.29 (m, 1H), 4.08 (s, 3H), 3.93 (s, 3H) ppm; ^{13}C NMR (100 MHz, DMSO-d_6): δ = 157.2, 146.3, 141.6, 138.2, 126.3, 124.0, 121.8, 120.9, 120.0, 116.6, 114.6, 112.9, 112.4, 110.5, 110.1, 93.1, 91.6, 56.5, 29.6 ppm; HRMS (ESI-MS): *m/z*: calcd for $C_{19}H_{13}N_4O$: 313.1084 $(M + H)^+$; found: 313.1090.

Synthesis of 4'-methoxy-2-nitro-1,1'-biphenyl (5)

A mixture of 1-bromo-2-nitrobenzene (4.27 g, 21.14 mmol), 4-methoxyphenylboronic acid (3.38 g, 22.24 mmol), $Pd(PPh_3)_4$ (1.22 g, 1.06 mmol) in 25 mL of aqueous K_2CO_3 2M and 30 mL of benzene under a nitrogen atmosphere was stirred at 90 °C for 2 h. Then, the mixture was cooled down to room temperature, treated with water and neutralized. The product was extracted with dichloromethane and the organic layer was dried over Na_2SO_4, filtered off and the solvent was distilled off under reduced pressure. The crude was purified by flash column chromatography by using a mixture of hexane and ethyl acetate (10:1 v/v) as the eluent to give compound **5** as a yellow solid (4.15 g; 86%). ^{1}H NMR (400 MHz, $CDCl_3$): δ = 7.80 (d, J = 8.0 Hz, 1H), 7.61-7.56 (m, 1H), 7.46-7.42 (m, 2H), 7.27-7.24 (m, 2H), 6.97-6.94 (m, 2H), 3.85 ppm (s, 3H).

Synthesis of 2-methoxy-9*H*-carbazole (6)

A mixture of **5** (3.95 g, 17.23 mmol) in 9 mL of triethyl phosphite was heated at 160 °C for 2 h. After cooling down to room temperature, hexane was added and the mixture was stirred for 10 min. The product was collected by suction filtration yielding compound **6** as a white solid (2.39 g; 70%). ^{1}H NMR (400 MHz, Acetone-d_6): δ = 10.18 (s, 1H), 7.99 (d, J = 7.8 Hz, 1H), 7.96 (d, J = 8.6 Hz, 1H), 7.44 (d, J = 8.1 Hz, 1H), 7.31-7.26 (m, 1H), 7.15-7.11 (m, 1H), 7.03 (d, J = 2.3 Hz, 1H), 6.81 (dd, J = 8.6 Hz, J = 2.3 Hz,

DOI: 10.1039/c6cp08078b

1H), 3.86 ppm (s, 3H); ^{13}C NMR (100 MHz, Acetone-d_6): δ = 160.1, 142.4, 141.0, 125.0, 124.2, 121.6, 120.0, 119.7, 117.7, 111.4, 108.8, 95.4, 55.7 ppm.

Synthesis of 2-methoxy-9-methyl-9*H*-carbazole (7)

NaH (445 mg, 11.13 mmol, 60% dispersion in mineral oil) was added to a solution of **6** (1.96 g, 9.94 mmol) in 18 mL of anhydrous DMF under a nitrogen atmosphere. The solution was stirred at room temperature for 30 minutes. Then, methyl iodide (693 µL, 11.13 mmol) was added and the mixture was stirred at room temperature for 30 minutes and then treated with water. The aqueous layer was extracted with dichloromethane and the organic layer was dried over Na_2SO_4, filtered off and the solvent was distilled off under reduced pressure. The crude was purified by flash column chromatography by using a mixture of hexane and dichloromethane (9:1 v/v) as the eluent to give compound **7** as a white solid (1.86 g; 89%). ^{1}H NMR (400 MHz, Acetone-d_6): δ = 8.01 (d, J = 7.8 Hz, 1H), 7.98 (d, J = 8.5 Hz, 1H), 7.46 (d, J = 8.2 Hz, 1H), 7.39-7.34 (m, 1H), 7.18-7.14 (m, 1H), 7.08 (d, J = 2.2 Hz, 1H), 6.82 (dd, J = 8.5 Hz, J = 2.2 Hz, 1H), 3.92 (s, 3H), 3.87 ppm (s, 3H); ^{13}C NMR (100 MHz, $CDCl_3$): δ = 159.3, 142.5, 141.2, 124.5, 123.1, 121.1, 119.5, 119.1, 116.8, 108.3, 107.4, 93.0, 55.8, 29.2 ppm.

Instrumentation and methods

Silica gel (SDS, 230-240 mesh) was used for flash column chromatography. ^{1}H NMR (400 MHz) and ^{13}C NMR (100 MHz) were collected on a Varian Mercury instrument. NMR spectra have been processed with the MestRe Nova software. Chemical shifts have been determined taking the signal of the solvent as the reference. High-resolution mass spectrometry (HR-MS) was performed on a LC/MSD-TOF Agilent Technologies apparatus by means of the electrospray (ESI-MS) technique. Single-crystal analyses were performed on a D8 Venture System equipped with a multilayer monochromator and a Mo microfocus (λ = 0.71073 Å). The frames were integrated with the Bruker SAINT software package using a narrow-frame algorithm. The structure was solved using the Bruker SHELXTL Software Package and refined using SHELXL.[15] Thermogravimetric analyses (TGA) were performed on a TA Instruments Q50 at a heating rate of 20 °C min^{-1} under nitrogen atmosphere. Differential scanning calorimetry (DSC) measurements were recorded on a TA Instruments Q2000 calorimeter at a scan rate of 10 °C min^{-1} under nitrogen atmosphere. UV-Vis spectra were registered in a Varian Cary UV-Vis-NIR 500E spectrophotometer. Cyclic voltammograms were carried out in a microcomputer-controlled potentiostat/galvanostat Autolab with PGSTAT30 equipment and GPES software. A cylindrical three-electrode cell was used. The reference electrode was a Ag/Ag^+ electrode (0.01 M $AgNO_3$ in acetonitrile). The counter and working electrodes were a platinum wire and a glassy-carbon electrode, respectively. All voltammetric curves were recorded under quiescent conditions, at a scan rate of 100 mV s^{-1} and under argon atmosphere. All solutions were prepared in dichloromethane (1 mM). Tetrabutylammonium hexafluorophosphate (0.1 M) was used as the supporting electrolyte. The ionization potential and electron affinity values were estimated from the onset of the first oxidation and reduction peaks, respectively, as IP = $E_{[\text{onset,ox vs. } Fc^+/Fc]}$ + 5.39 and EA = $E_{[\text{onset,red vs. } Fc^+/Fc]}$ + 5.39, where 5.39 eV corresponds to the formal potential of the Fc^+/Fc couple in the Fermi scale.[16]

TOF measurements. The samples for the TOF measurements were prepared by the thermal vacuum evaporation technique with a base pressure below 10^{-6} mbar. The layers of the compounds were deposited on pre-cleaned indium tin oxide (ITO) coated glass substrates with the thicknesses in the range of 0.8-5.0 µm followed by deposition of 80 nm of aluminium using a mask. The thickness of the organic layers was measured with a profilometer. The area of the obtained devices was 0.06 cm^2. Photo generation of charge carriers was carried out by light pulse through the ITO. For hole mobility measurements positive voltage was applied to the ITO electrode, whereas for electron mobility measurements negative voltage was applied. A Keithley 6517B electrometer was used to apply external voltages with a pulsed third-harmonic Nd:YAG laser EKSPLA NL300 working (pulse duration was 3-6 ns, wavelength 355 nm). A digital storage oscilloscope Tektronix TDS 3032C was used to record the TOF transients. The transit time (t_t) was determined by the kink on the curve of the transient in the log–log scale. The drift mobility (μ) was calculated by the formula $\mu = d^2/Ut_t$, where d is the layer thickness and U is the surface potential at the moment of illumination.

Details of theoretical calculations

All structures were optimized and the molecular orbitals were generated by using density function theory (DFT) semi-local hybrid functional B3LYP and 6-31+G(d) basis set with a diffusion function (+). The electrostatic potential map (EPM) at the same level of theory was calculated in order to understand the electron density and the strength of the bonding interactions present in the molecules. The rotation probability of the tricyanovinyl moiety and the single point energies of compounds **3** and **4** were analysed via the theoretical potential energy scan experiment using the same level of theory, where rotation steps of 20° were used. The intermolecular interaction energies between molecules for compounds **3** and **4** were estimated using the basis set superposition effect (BSSE) concept and at wB97X-D functional with the London dispersion corrections and 6-311G(d) basis set.[17] The dimers of molecules from X-ray analysis were generated. For the intermolecular interactions visualization, the Mercury 3.7 program was used. The Marcus theory[18] (equation 1) was used to determine the rate of charge transfer between molecules:

DOI: 10.1039/c6cp08078b

$$k_i = \frac{2\pi}{\hbar} |H_i|^2 \frac{1}{\sqrt{4\pi\lambda k_b T}} \exp\left(-\frac{(\lambda+\Delta G^0)^2}{4\lambda k_b T}\right) \times \exp\left(-\frac{eFd_i}{\varepsilon k_b T}\right) \qquad (1)$$

where k_i is the electron transfer rate constant for pathway i, H_i is the electronic coupling between the initial and final states, λ is the internal reorganization energy, ΔG^0 is the total Gibbs free energy of change for the charge transfer reaction, k_b is the Boltzmann constant and T is the absolute temperature (298 K). However, the influence of the electric field on the activation energy from Marcus theory (i.e. on $E_a = (\lambda + \Delta G^0)^2 / (4\lambda)$ but not on ΔG^0) was proposed. In support of this idea, Pivrikas et al.[19] showed that the electric field has an impact on the activation energy of electron transport in fullerene diodes. This model showed a good agreement with the experimental data in our previous work.[20] In this exponential component, e is the elementary charge (1.60×10^{-19} C), F is the applied external electric field, ε is the dielectric constant (permittivity) of the material and d_i is the distance for pathway i between neighbouring donor-donor (D-D) for holes and acceptor-acceptor (A-A) moieties for electrons. The dielectric constants ε (permittivities) of **3** and **4** materials were estimated according to the Clausius-Mossotti equation (2)[21,22] which expresses the dielectric constant as:

$$\varepsilon = \left(1 + \frac{8\pi\alpha}{3V}\right) \times \left(1 - \frac{4\pi\alpha}{3V}\right)^{-1} \qquad (2)$$

where α is the isotropic polarizability and V is the molecular volume plus the Van der Waals radius of 1Å. The isotropic polarizability was calculated by the B3LYP/6-31+G(d) method. The ε values were estimated to be 3.4 and 3.2 for **3** and **4** materials, respectively. These data show a good correlation with data from literature. Traditionally, the organic materials are characterized by low ε (i.e. 2-7) in the solid state.[23] However, the influence of the electric field on ε was ignored to simplify the modelling. The calculated parameters are provided in Table S4 of the Supporting Information.

On the other hand, the charged sites are polarized by its surrounding environment and an external electric field, which in turn would cause an additional energy shift.[24,25] Therefore, ΔG^0 is the energy deference of the initial and final state of the charge transfer process. The Gibbs free energy was approximated to equation (3):

$$\Delta G^0 = -eF\varepsilon^{-1}d_i - P^{\pm} \qquad (3)$$

where $P^{\pm}$ is the polarization energy for holes and electrons, respectively. The polarization energy (P^+ and P^-) measures the contribution of intermolecular interactions in the solid state to hole and electron transport levels and includes both the electrostatic and polarization contributions. The $P^{\pm}$ energies are defined as the difference between the solid state and gas phase values of ionization potential and electron affinity, respectively.[26] The crystal cells of 3 and 4 were used for estimation of the vertical ionization potentials (IP) and electron affinities (EA) by using the B3LYP/6-31+G(d) method in the solid state. The polarization energies for one dimension can be described by the formula $P^+ = \frac{1}{3}(IP_{cryst} - IP_{gas})$ or $P^- = \frac{1}{3}(EA_{cryst} - EA_{gas})$, respectively for holes and electrons.[27] The values (P^+ and P^-) were estimated to be (-0.24, -0.20 eV) and (-0.24, -0.25 eV) for 3 and 4, respectively.

From the literature, the computed values of external reorganization energy are very small compared to the internal reorganization energy component (i.e. typically lower than about 9 meV).[28] Moreover, the values of internal reorganization energy for the modelled compounds were calculated by the adiabatic potential energy surface method[29] and at the B3LYP/6-31+G(d) level in vacuum according to equation (4):

$$\lambda = [E^{\pm}(g^0) - E^{\pm}(g^{\pm})] + [E^0(g^{\pm}) - E^0(g^0)] \qquad (4)$$

In this equation, E corresponds to the energy of the neutral molecule (g^o) in the geometry of cationic/anionic species ($g^{\pm}$), respectively.

The coupling integrals are one of the key parameters determining charge carrier mobility. The integrals H_i for the pathways (see Figure 5 and Supporting Information) between molecules m and n were obtained by the site-energy overlap correction method (5)[30] at the long-range corrected hybrid density functional wB97X-D and 6-311G(d) basis set in *vacuum.*

$$H_i = \frac{H_{mn}^0 - \frac{1}{2}S_{mn}(H_{mm}+H_{nn})}{1-S_{mn}^2} \qquad (5)$$

where H_{mn}^0 is the electronic coupling (transfer) matrix element, S_{mn} is the overlap integral, and $H_{mm(nn)}$ are the energies of the neutral and charged dimer states.

The diffusion coefficient (D) for all migrations of electrons or holes between neighbouring molecules is given by the Pauli master equation[31] (6):

$$D = \frac{1}{2N}\sum_i d_i^2 k_i p_i \qquad (6)$$

where N is the dimensionality (N=3) and d_i is the distance between the neighboring D-D for holes and A-A moieties for electrons in dimer i, and p_i is a probability of charge migration. The molecular dynamics (Monte Carlo) simulations based on the empirical force fields can be used to obtain a well-equilibrated amorphous structure of the organic solids.[32] However, the energies of intermolecular interactions are not considered in this method and the injection sites with equal probability are used. Taking into account the intermolecular interactions, the probability of sites can be estimated by using Boltzmann distribution depending on the intermolecular interaction energy difference ΔE_i and temperature.[20] The evolution equation (7) for p_i is given by:

$$p_i = \frac{k_i}{\sum_i k_i} \times \frac{\exp\left(-\frac{\Delta E_i}{k_b T}\right)}{\sum_i \exp\left(-\frac{\Delta E_i}{k_b T}\right)} \qquad (7)$$

The final drift mobility (μ) was calculated according to the Einstein equation (8) using the single-step approximation:

$$\mu = \frac{e \cdot D}{k_b T} \qquad (8)$$

All DFT calculations were done with the Spartan'14 program in vacuum and at 298K.[33]

Acknowledgements

Financial support from the *Ministerio de Economía y Competitividad* (CTQ2015-65770-P MINECO/FEDER) is gratefully acknowledged. This work was also partially supported by H2020-ICT-2014/H2020-ICT-2014-1 project PHEBE (grant agreement No 641725).

Keywords: Carbazole • Tricyanovinylene • Charge transfer • Semiconductors • DFT calculations

[1] Y. Shirota, H. Kageyama, *Chem. Rev.* **2007**, *107*, 953-1010.
[2] a) W. Yue, T. He, M. Stolte, M. Gsänger, F. Würthner, *Chem. Commun.* **2014**, *50*, 545-547; b) Y. Zhang, C. Kim, J. Lin, T.-Q. Nguyen, *Adv. Funct. Mater.* **2012**, 22, 97-105; c) Z. Liang, Q. Tang, R. Mao, D. Liu, J. Xu, Q. Miao, *Adv. Mater.* **2011**, *23*, 5514; d) S. Fabiano, H. Wang, C. Piliego, C. Jaye, D. A. Fischer, Z. Chen, B. Pignataro, A. Facchetti, Y.-L. Loo, M. A. Loi, *Adv. Funct. Mater.* **2011**, *21*, 4479-4486.
[3] a) L. Dou, Y. Liu, Z. Hong, G. Li, Y. Yang, *Chem. Rev.* **2015**, *115*, 12633-12665; b) X. Gao, Y. Hu, *J. Mater. Chem. C* **2014**, 2, 3099-3117; c) Y. Zhao, Y. Guo, Y. Liu, *Adv. Mater.* **2013**, *25*, 5372-5391.
[4] a) S. Banerjee, F. Ali, P. K. Nayak, N. Agarwal, *Thin Solid Films* **2012**, *520*, 2644-2650; b) J. L. Díaz, A. Dobarro, B. Villacampa, D. Velasco, *Chem. Mater.* **2001**, *13*, 2528-2536.
[5] a) A. Wojciechowski, M. M. M. Raposo, M. C. R. Castro, W. Kuznik, I. Fuks-Janczarek, M. Pokladko-Kowar, F. Bures, *J. Mater. Sci.: Mater. Electron.* **2014**, *25*, 1745-1750; b) S. Rodríguez González, J. Orduna, R. Alicante, B. Villacampa, K. A. McGee, J. Pina, J. Seixas de Melo, K. M. Schwaderer, J. C. Johnson, B. A. Blackorbay, J. J. Hansmeier, V. F. Bolton, T. J. Helland, B. A. Edlund, T. M. Pappenfus, J. T. López Navarrete, J. Casado, *J. Phys. Chem. B* **2011**, *115*, 10573-10585.
[6] a) Y. A. Getmanenko, T. A. Purcell, D. K. Hwang, B. Kippelen, S. R. Marder, *J. Org. Chem.* **2012**, *77*, 10931-10937; b) X. Cai, M. W. Burand, C. R. Newman, D. A. da Silva Filho, T. M. Pappenfus, M. M. Bader, J.-L. Bredas, K. R. Mann, C. D. Frisbie, *J. Phys. Chem. B* **2006**, *110*, 14590-14597.
[7] a) E. C.-H. Kwok, D. P.-K. Tsang, M.-Y. Chan, V. W.-W. Yam, *Chem. Eur. J.* **2013**, *19*, 2757-2767; b) P. Qin, J. Wiberg, E. A. Gibson, M. Linder, L. Li, T. Brinck, A. Hagfeldt, B. Albinsson, L. Sun, *J. Phys. Chem. C* **2010**, *114*, 4738-4748.
[8] a) M. Reig, J. Puigdollers, D. Velasco, *J. Mater. Chem. C* **2015**, *3*, 506-513; b) A. Tomkeviciene, J. V. Grazulevicius, D. Volyniuk, V. Jankauskas, G. Sini, *Phys. Chem. Chem. Phys.* **2014**, *16*, 13932-13942; c) N. Drolet, J.-F. Morin, N. Leclerc, S. Wakim, Y. Tao, M. Leclerc, *Adv. Funct. Mater.* **2005**, *15*, 1671-1682.
[9] J.-F. Morin, M. Leclerc, D. Adès, A. Siove, *Macromol. Rapid. Commun.* **2005**, *26*, 761-778.
[10] a) A. Tomkeviciene, J. V. Grazulevicius, K. Kazlauskas, A. Gruodis, S. Jursenas, T.-H. Ke, C.-C. Wu, *J. Phys. Chem. C* **2011**, *115*, 4887-4897; b) S. Castellanos, V. Gaidelis, V. Jankauskas, J. V. Grazulevicius, E. Brillas, F. López-Calahorra, L. Julià, D. Velasco, *Chem. Commun.* **2010**, *46*, 5130-5132.
[11] a) D.-Y. Goo, S. K. Woo, *Org. Biomol. Chem.* **2016**, *14*, 122-130; b) V. Arun, P. O. V. Reddy, M. Pilania, D. Kumar, *Eur. J. Org. Chem.* **2016**, 2096-2100; c) J. H. Smitrovich, I. W. Davies, *Org. Lett.* **2004**, *6*, 533-535.

DOI: 10.1039/c6cp08078b

[12] G. Bubniene, T. Malinauskas, M. Daskeviciene, V. Jankauskas, V. Getautis, *Tetrahedron* **2010**, *66*, 3199-3206.
[13] V. Vaissier, J. M. Frost, P. R. F. Barnes, J. Nelson, *J. Phys. Chem. C* **2015**, *119*, 24337-24341.
[14] E. G. Popova, L. A. Chetkina, B. V. Kotov, *Zhurnal Strukturnoi Khimii*, **1981**, *22*, 116-120.
[15] G. M. Sheldrick, *Acta Cryst*. **2008**, *A64*, 112-122.
[16] a) C. M. Cardona, W. Li, A. E. Kaifer, D. Stockdale, G. C. Bazan, *Adv. Mater*. **2011**, *23*, 2367-2371; b) A. J. Bard, L. R. Faulkner, *Electrochemical Methods: Fundamentals and Applications*, WILEY-VCH, New York, **2001**.
[17] F. Biedermann, H.-J. Schneider, *Chem. Rev*. **2016**, *116*, 5216-5300.
[18] R. A. Marcus, *Angew. Chem. Int. Ed. Engl*. **1993**, *32*, 1111-1121.
[19] A. Pivrikas, M. Ullah, H. Sitter, N. S. Sarisiftci, *Appl. Phys. Lett*. **2011**, *98*, 092114/1-3.
[20] G. Bagdziunas, G. Grybauskaite, N. Kostiv, K. Ivaniuk, D. Volyniuk, A. Lazauskas, *RSC Adv*. **2016**, *6*, 61544-61554.
[21] A. Natan, N. Kuritz, L. Kronik, *Adv. Funct. Mater*. **2010**, *20*, 2077-2084.
[22] H. M. Heitzer, T. J. Marks, M. A. Ratner, *J. Am. Chem. Soc*. **2015**, *137*, 7189-7196.
[23] W. Volksen, R. D. Miller, G. Dubois, *Chem. Rev.* **2010**, *110*, 56-110.
[24] M. Schwarze, W. Tress, B. Beyer, F. Gao, R. Scholz, C. Poelking, K. Ortstein, A. A. Günther, D. Kasemann, D. Andrienko, K. Leo, *Science* **2016**, *352*, 1446-1449.
[25] N. Ueno, *Science* **2016**, *352*, 1395-1396.
[26] S. M. Ryno, C. Risko, J.-L. Brédas, *ACS Appl. Mater. Interfaces* **2016**, *8*, 14053-14062.
[27] A. Bucinskas, G. Bagdziunas, A. Tomkeviciene, D. Volynyuk, N. Kostiv, D. Gudeika, V. Jankauskas, M. Rutkis, J. V. Grazulevicius, *RSC Adv*. **2015**, *5*, 49577-49589.
[28] D. P. McMahon, A. Troisi, *J. Phys. Chem. Lett*. **2010**, *1*, 941-946.
[29] M. Malagoli, J. L. Brédas, *Chem. Phys. Lett*. **2000**, *327*, 13-17.
[30] Z. Shuai, H. Geng, W. Xu, Y. Liao, J.-M. André, *Chem. Soc. Rev*. **2014**, *43*, 2662-2679.
[31] Y. Olivier, V. Lemaur, J. L. Brédas, J. Cornil, *J. Phys. Chem. A* **2006**, *110*, 6356-6364.
[32] H. Bässler, *Phys. Stat. Sol. B* **1993**, *175*, 15-56.
[33] Spartan'14 for Windows Version 1.1.2. 1840 Von Karman Avenue, Suite 370, Irvine, CA